

Recognition of Lung Nodules in Computerized Tomography Lung Images using a Hybrid Method with Class Imbalance Reduction

Yingqiang Wang, Honggang Wang, Erqiang Dong*

School of Electronic Information Engineering, Xi'an Siyuan University
Xi'an 710038, Shaanxi, China

Abstract—Lung cancer is among the deadly diseases affecting millions globally every year. Physicians' and radiologists' manual detection of lung nodules has low efficiency due to the variety of shapes and nodule locations. The paper aims to recognize the lung nodules in computerized tomography (CT) lung images utilizing a hybrid method to reduce the problem space at every step. First, the suggested method uses the fast and robust fuzzy c-means clustering method (FRFCM) algorithm to segment CT images and extract two lungs, followed by a convolutional neural network (CNN) to identify the sick lung for use in the next step. Then, the adaptive thresholding method detects the suspected regions of interest (ROIs) among all available objects in the sick lung. Next, some statistical features are selected from every ROI, and then a restricted Boltzmann machine (RBM) is considered a feature extractor that extracts rich features among the selected features. After that, an artificial neural network (ANN) is employed to classify ROIs and determine whether the ROI includes nodules or non-nodules. Finally, cancerous ROIs are localized by the Otsu thresholding algorithm. Naturally, sick ROIs are more than healthy ones, leading to a class imbalance that substantially decreases ANN ability. To solve this problem, a reinforcement learning (RL)-based algorithm is used, in which the states are sampled. The agent receives a larger reward/penalty for correct/incorrect classification of the examples related to the minority class. The proposed model is compared with state-of-the-art methods on the lung image database consortium image collection (LIDC-IDRI) dataset and standard performance metrics. The results of the experiments demonstrate that the proposed model outperforms its rivals.

Keywords—Lung cancer; artificial neural network; fuzzy c-means clustering method; reinforcement learning; restricted boltzmann machine

I. INTRODUCTION

Lung cancer is a dangerous and deadly disease, causing millions of deaths worldwide each year. The chances of surviving for five years with lung cancer are only 14% [1, 2]. CT imaging is the most popular method for screening lung nodules and has reduced lung cancer mortality by 20% [3]. CT provides valuable information for the diagnosis of lung cancer, but as the number of images increases, accurate evaluation becomes more challenging and poses risks to radiologists [4]. Therefore, it has become necessary to assist physicians in making faster and more accurate decisions than CT images [5].

Various methods are used for lung segmentation, including supervised, unsupervised, and semi-supervised learning

approaches. Supervised learning techniques such as ANN require training data to provide good performance for segmentation [6]. Deep neural networks are becoming popular but require large training datasets and huge computational costs [7]. Unsupervised learning approaches, such as clustering-based methods, rely on the entire image and operate based on the acquired pixel distances. Partitional and hierarchical clustering techniques are primary examples of cluster analysis, with crisp and fuzzy clustering procedures as subcategories [8]. The fuzzy c-means (FCM) algorithm is superior to other clustering algorithms because it is more tolerant of ambiguity and retains more of the image, but it struggles to segment images containing complex textures and backgrounds. Boosted clustering algorithms have been employed to segment lung nodules, but they suffer from sensitivity to noise and require a lot of repetition for convergence. The FRFCM segmentation algorithm [9] is suggested to segment nodules from lung CT images with strategic views of robustness against noise and more rapid but precise segmentation performance. The FRFCM algorithm defines a spatial function by combining the similarity of the gray pixel value and the membership to update the membership function in each iteration. The FRFCM algorithm can provide suitable segmentation results for all images with low computational cost and high accuracy.

Esfandiari et al. [10] conducted a systematic review of medical studies and found that categorization is the most time-consuming aspect of data mining approaches in medical fields such as diagnosis, therapy, and screening. Meanwhile, Lee et al. [11] studied methods for identifying lung nodules and found that most of them relied on the classification of nodule candidates, which reduces workload by removing undesirable portions from CT images. Adaptive thresholding-based methods are considered the most effective for identifying lung nodule candidates, although various other methods have been utilized [12]. The most successful image classification models, including medical ones, are CNNs. However, using CNNs for nodule candidate classification cannot achieve high performance since they are not suitable for extracting features from images with low dimensions [13].

RBMs [14] are a variety of neural networks with stochastic processing units coupled bi-directionally. Two classes of neurons are visible and hidden in an RBM. A group of neurons has no connection between its nodes, yet it must nonetheless form a bipartite network with symmetric connections between

*Corresponding Author.

its visible and hidden units. RBMs can be trained using more effective algorithms than unrestricted Boltzmann machines. In classification applications, RBMs are frequently used for feature extraction [15].

Data imbalance, which can significantly reduce performance, is a major challenge to medical image classification, as negative instances are much smaller than positive ones. Measures that could be implemented to contend with class imbalance are separated into algorithm-level and data-level methods. The data-level strategy uses under-sampling, over-sampling, or a combination of the two to lessen the negative consequences of imbalanced classification [16]. Algorithm-level approaches increase the weight of the minority class [17]. Furthermore, deep-learning approaches could be employed to address the issue of imbalanced classification [18]. Over recent years, various domains, such as computer games, robots' control, and recommendation systems, have successfully employed deep reinforcement learning (DRL). DRL enhances the performance of classification problems by eliminating noisy data and discovering better features. Notwithstanding, few works have applied DRL to classify imbalanced data. DRL is eminently suitable for classifying imbalanced data because of its learning approach. It employs a reward function that discriminates between classes by imposing heavier penalties on minority classes or giving higher rewards to them.

The paper presents a hierarchical lung nodule detection model established on the FRFCM clustering algorithm, an RBM, and an ANN boosted by a RL-based algorithm. The proposed model includes five steps, which is shown in Fig. 1: 1) Patient lung extractor: The FRFCM algorithm is used to segment CT images into two right and left lungs, followed by the utilization of a CNN to identify sick lungs. 2) Nodule candidate detection: In this step, an adaptive thresholding algorithm is employed to recognize the suspected region of interest (ROI). 3) Feature extraction: Some standard features are selected from every ROI, and then the RBM is considered as a feature extractor that extracts rich features among the standard features. 4) Classification: The features extracted by RBM are entered into an ANN to classify ROIs as healthy or sick areas. Due to many healthy areas than sick ones, ANN becomes imbalanced. RL is used to solve this issue and describe classification as a guessing game with sequential decision-making steps. At each stage, the agent uses a training instance to represent the environmental state and then, guided by a policy, performs a three-class classification operation. The classifier will accept a positive reward if the operation is completed; a negative reward will be given. The minority class receives higher compensation than the majority class. The agent's objective is to categorize the samples as precisely as possible to earn the most cumulative rewards, and 5) Localization of nodules: The Otsu thresholding algorithm is used to localize the nodule.

The contributions of the suggested model can be summed up as follows: 1) A hybrid model is presented that contains some steps that try to decrease the problem space in every step, 2) The FRFCM algorithm is considered for segmentation, which is one developed model with low computational cost and high accuracy, 3) A DRL model is offered for the classification

problem of ROIs to address imbalanced classification, and 4) The effectiveness of each component, including lung segmentation, classification, and nodule identification, is examined through studies, and its performance is evaluated in comparison to other approaches.

The remaining sections of the article are structured as follows: In Section II, a review of the literature for analyzing the lung nodule is provided. In Section III, the suggested approach is presented in further depth. Section IV presents the experimental findings and necessary analyses. Section V presents the discussion. Finally, the conclusion of the paper is presented in Section VI.

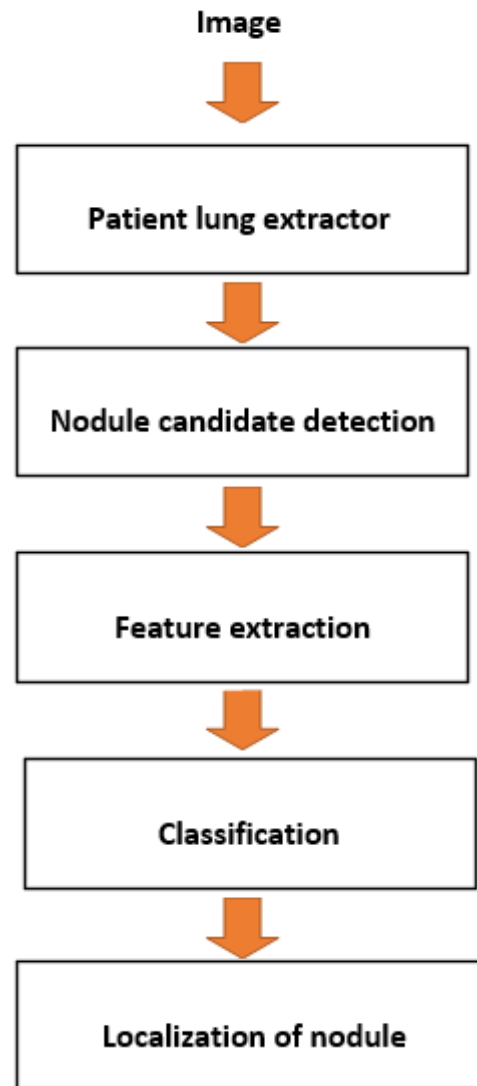


Fig. 1. Steps of the proposed algorithm.

II. RELATED WORK

Due to the small size of nodules, interpreting the CT images by the radiologist becomes difficult, so the task of accurate diagnosis is in trouble [19]. On the other hand, early detection of nodules is essential to achieve the best treatment plan and increase the survivability rate [20]. So far, many types of machine learning and deep learning approaches have been

introduced, focusing on detecting and localizing lung nodules, some of which are reviewed in this section.

A. Machine Learning

Ozekes and Camurcu [21] presented an automatic approach for pulmonary nodule detection using traditional machine learning methods like template matching. Wu, Sun, Wang, Li, Wang, Huo, Lv, He, Wang and Guo [22] designed an ANN architecture to distinguish malignant from benign samples. Texture and radiologist features were extracted and combined for classification in this work. Kuruvilla and Gunavathi [23] presented a computer-aided design (CAD) system comprising segmentation and classification stages for CT images. First, segmentation was done, then extracting features from the segmented area. Finally, an ANN was hired for classification. This work considered conventional features such as mean, SD, and skewness. Farahani, Ahmadi and Zarandi [24] founded a CAD system to diagnose pulmonary nodules in CT images. Their algorithm included three steps. First, a new segmentation algorithm was proposed based on FCM and KFCM algorithms that achieved acceptable results for lung segmentation. Second, they manually analyzed features and selected the best one for nodules classification. Finally, an ensemble of classifiers was applied for classification. Khan, Rubab, Kashif, Sharif, Muhammad, Shah, Zhang and Satapathy [25] combined pre-processing step with an ensemble approach for localized lung cancer. They showed that contrast stretching integrated with the discriminative classical features and the ensemble classifier could achieve high performance.

The inflexibility of feature extraction strategy is a major challenge in machine learning, particularly in deep learning. The lack of flexibility makes it difficult to learn high-level representations that generalize well to new and unseen data. This is particularly problematic when working with complex and heterogeneous datasets, where feature extraction is often a time-consuming and computationally expensive process. In addition, inflexible feature extraction strategies can also lead to overfitting, where the model becomes too specialized to the training data and performs poorly on new data.

B. Deep Learning

With the advent of deep learning algorithms in many applications [26-38], many researchers used them for nodule detection tasks [39, 40]. With its layered structure, deep learning can learn high-level features with high accuracy [41, 42]. Zhang, Yang, Gong, Jiang and Wang [43] introduced fusion feature vectors that integrated CNN, LBP, and HOG features to characterize the nodule area better. They used deep learning as a feature extraction module, in which the final feature vector was passed to a GBM classifier. The proposed method employed hybrid features for lung nodule classification. Hu et al. [61] combined the K-means algorithm kernel with the Mask R-CNN deep segmentation technique. This study had the greatest results, with a segmentation accuracy of 97% and an average runtime of 11s. Blanc et al. [44] offered a method to classify pulmonary nodules into two classes depending on whether their volume is greater than 100 mm³ or not. Zhang et al. [45] presented a multi-level CNN method to extract the essential features of any image. They optimize the values of meta-parameters using a non-stationary

kernel-based Gaussian surrogate model. Mobiny and Van Nguyen [46] developed an algorithm based on capsule networks for 3D lung nodules. The authors have shown that their algorithm performs well when a small dataset size. However, the prediction accuracy decreases when the dataset becomes too large. Kim et al. [47] designed a method based on the multi-scale gradual integration CNN, which used multi-scale inputs with different levels for classification. The proposed classification method suffers from data imbalance. Ozdemir et al. [48] suggested a two-step Bayesian CNN structure to take advantage of the segmentation predictions and uncertainties. In the first one, segmentation algorithms were performed on 2D axial CT slices. The original image combines segmentation predictive mean and standard deviation maps to create a 3-channel composite image fed into a 3D Bayesian CNN for nodule detection. Zhu et al. [49] combined expectation maximization (EM) to make a new 3D CNN method, whose purpose was to extract poorly supervised labels for nodule detection. In this algorithm, the Faster RCNN algorithm completed the nodule suggestion generation. Moreover, Logistic regression and the Half-Gaussian model were used for the central lobe location slice. Dou et al. [50] incorporated a group of 3D CNNs with diverse receptive field sizes to use multi-level contextual data around nodules. There are three different 3D CNNs designed for different-sized cropped cubes. Jiang et al. [51] suggested employing multi-group patches extracted from lung scans as a method for lung nodule detection. Frangi-filters were first utilized to remove the vessel-like formations. A slope analysis method was created to remove the nodules from the lung by enhancing the juxta-pleural nodules. Eventually, a CNN using multi-crop (MC) pooling was created to understand the specifics of radiologists using original CT images and their binarization. Dodia et al. [52] developed a new deep-learning-based method to detect lung nodules with decreased false positives. Their work employs a receptive regularization on the convolution and deconvolution layers of a decoder block in the V-Net. Huang et al. [53] proposed a CAD-based method that utilizes a 3D CNN [54] to detect lung nodules in low-dose CTs. The proposed method merges a priori intensity and geometrical knowledge about nodules and complicates anatomical structures with features and classifiers. Wu et al. [55] presented an interpretable method for pulmonary nodule segmentation, which supplies high-level semantic attributes and the areas of detected nodules. Huang et al. [56] introduced a fast and fully-automated end-to-end approach that automatically segments the exact nodule contours from the raw CT images with few FPs. Maqsood et al. [57] conducted a segmentation method using U-Net for lung nodule segmentation. Their technique increased the view of filters without reducing the loss and scope of data by integrating compactly and densely linked useful convolutional blocks with Atrous convolution blocks. Shen et al. [58] proposed a methodology called MC-CNN, which automatically obtains important nodule information by employing a multi-crop pooling strategy, cropping different regions from convolutional feature maps, and then repeatedly utilizing max-pooling.

Although deep models benefit from some properties, including extracting automatic features, they suffer from several difficulties. In the case of lung segmentation, an

extensive training dataset and huge computational costs are required for deep learning models. In nodule detection, they extract some suspicious ROIs and then classify them using CNN-based methods. Even though CNN can extract rich features, they fail in extracting features from small areas, i.e., ROIs.

III. ARCHITECTURE OF THE PROPOSED APPROACH

The paper offers a hybrid model containing steps that decrease problem space at every step. The proposed model consists of five steps: Patient lung extractor, Nodule candidate detection, Feature extraction, Classification, and Extraction of nodule area. First, CT images are segmented by the FRFCM algorithm that extracts two lungs, and then the lung containing the nodule for the next steps is identified by a CNN. In the second step, the adaptive thresholding method is hired to recognize ROIs from the suspicious lung. In the third step, some standard features from every ROI are selected, and then an RBM is considered to extract rich features from the standard ones. After that, the features extracted by RBM into an ANN to classify ROIs as healthy or sick areas. The proposed ANN benefits from an RL-based algorithm to handle class imbalance. Finally, the Otsu thresholding algorithm is used to localize the nodule. The overall architecture of the suggested model is given in Fig. 2; the next section provides further specifics.

A. Patient Lung Extractor

This step aims to segment the lungs of a CT image to reduce the search space by removing backgrounds and noises. The literature survey has proposed many preliminary segmentation methods for lung segmentation, but most fail to remove the noise from the image and segmentation quickly. To improve the weakness of the FCM-related algorithms, which are sensitive to noise, the FRFCM algorithm was proposed by combining local spatial data into the FCM algorithm to get better precision results. The objective function of the FCM algorithm with local information is provided by

$$J_m = \sum_{i=1}^N \sum_{k=1}^c u_{ki}^m ||x_i - v_k||^2 + \sum_{i=1}^N \sum_{j=1}^c G_{ki} \quad (1)$$

where $f = \{x_1, x_2, \dots, x_N\}$ illustrates a grayscale image, where x_i stands for the gray level of the i -th pixel. N shows the total number of pixels in image f , and c displays the number of clusters. m indicates a weighting exponent on each fuzzy membership, determining the amount of fuzziness of the resultant classification. $U = [u_{ki}]$ and G_{ki} denote the membership partition matrix and fuzzy factor provided as

$$G_{ki} = \sum_{\substack{r \in N_i \\ i \neq r}} \frac{1}{d_{ir} + 1} (1 - u_{kr})^m ||x_r - v_k||^2 \quad (2)$$

$$u_{ki} = \frac{1}{\sum_{j=1}^c \left(\frac{||x_i - v_k||^2 + G_{ki}}{||x_i - v_j||^2 + G_{ji}} \right)^{\frac{1}{m-1}}} \quad (3)$$

where v_k describes the prototype value of the k -th cluster, computed as

$$v_k = \frac{\sum_{i=1}^N u_{ki}^m x_i}{\sum_{i=1}^N u_{ki}^m} \quad (4)$$

Additionally, regarding morphological reconstruction (MR), the reconstruction of an image is shown as d and provided by

$$\varepsilon_p = R_e^c(f) \quad (5)$$

where $R_e^c(\cdot)$ is the morphological closing reconstruction, which is calculated as

$$R_e^c(f) = R_{R_f^\beta(\tau(f))}^\tau(\beta(R_f^\beta(\tau(f)))) \quad (6)$$

where τ and β stand for the erosion and dilation operation, respectively. Finally, considering morphological closing reconstruction, the objective function of FRFCM is computed as

$$J_m = \sum_{k=1}^c \sum_{p=1}^q [u_{kp}^m (||\varepsilon_p - v_k||)^2] + \sum_{k=1}^c \sum_{p=1}^q G_{kp} \quad (7)$$

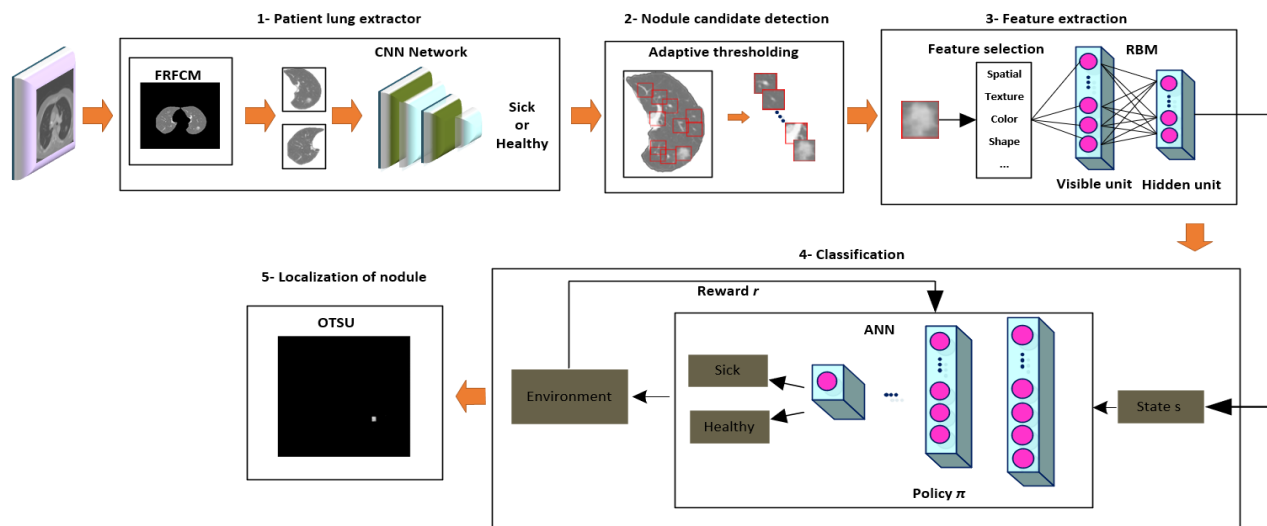


Fig. 2. Overall architecture of the proposed model.

A CNN is used to identify the lung containing nodules to decrease the search space further. Specifically, the only purpose of using CNN is to determine which lung in the CT image has the nodule, regardless of the nodule position.

B. Nodule Candidate Detection

The presence of any pulmonary nodules must be determined after the ill lung has been located using CT scans. However, finding nodules is difficult because pulmonary nodules are predominantly linked to the pleura or blood vessels. Moreover, various structural structures, such as blood arteries, airways, bronchioles, and alveoli, are present in both lungs and may have a comparable gray level to the nodules. Therefore, a transition step is needed to avoid missing nodules in CT images to specify a set of possible nodule candidates from ROIs [59]. This paper applies the adaptive thresholding method [61], one of the most valuable and efficient thresholding techniques, to select pulmonary nodule candidates for segmented lung images. This algorithm selects pixels less than a threshold value (TV) as the background, and those higher than the TV are chosen as the nodule candidate areas. In this method, the TV of each pixel is established on the values of the adjacent pixel intensity. The output of this step is different regions where the nodule is likely to be present. In this article, the bounding box, which has the most intersection of union (IOU) [60] with the actual location of the nodule, is identified as the patient area. Furthermore, two bounding boxes with IoU = 0 are randomly selected as non-nodule regions.

C. Feature Extraction

After detecting the nodule candidates from the sick lungs, the following stage selects a comprehensive feature vector for

each ROI to distinguish them as nodule or non-nodule. Indeed, ROIs and other structures are classified on such feature vectors. Although CNNs can select and extract automatically, they suffer from the classification of low dimensions, i.e., ROIs [61]. In this study, six classes of statistical features are used [62]: 1) Spatial including Entropy, Mean, Kurtosis, Skewness, Histogram of Oriented Gradients (Hog), 2) Texture including Haralick, Local Binary Pattern (LBP), Gray Level Co-occurrence Matrix (GLCM), Oriented FAST and Rotated BRIEF (ORB), 3) Color including Min Intensity, Max Intensity, Mean Intensity, Weighted Intensity, 4) Shape containing Area, Perimeter, Extent, Solidity, 5) Transform including Orientation, and 6) Edge including Corner Harries. These features are the most important ones that paraphrase an area appropriately. Fig. 3 shows the placement of these features in a vector for the next step.

It is possible that some features selected may be irrelevant and redundant, so a feature extraction step seems necessary. Many medical applications, particularly classification, depend on feature extraction [63]. It extracts the most relevant features and preserves the important information of the original image by removing unrelated and repetitious information [64]. An RBM is used that extracts efficient features and reduces the feature vector for this goal. Structurally, RBM is a deep architecture consisting of two layers of stochastic units called visible and hidden. Each element in the unit is connected indirectly with all pairs of another unit. There are no connections from visible to visible or hidden to hidden nodes in an RBM.

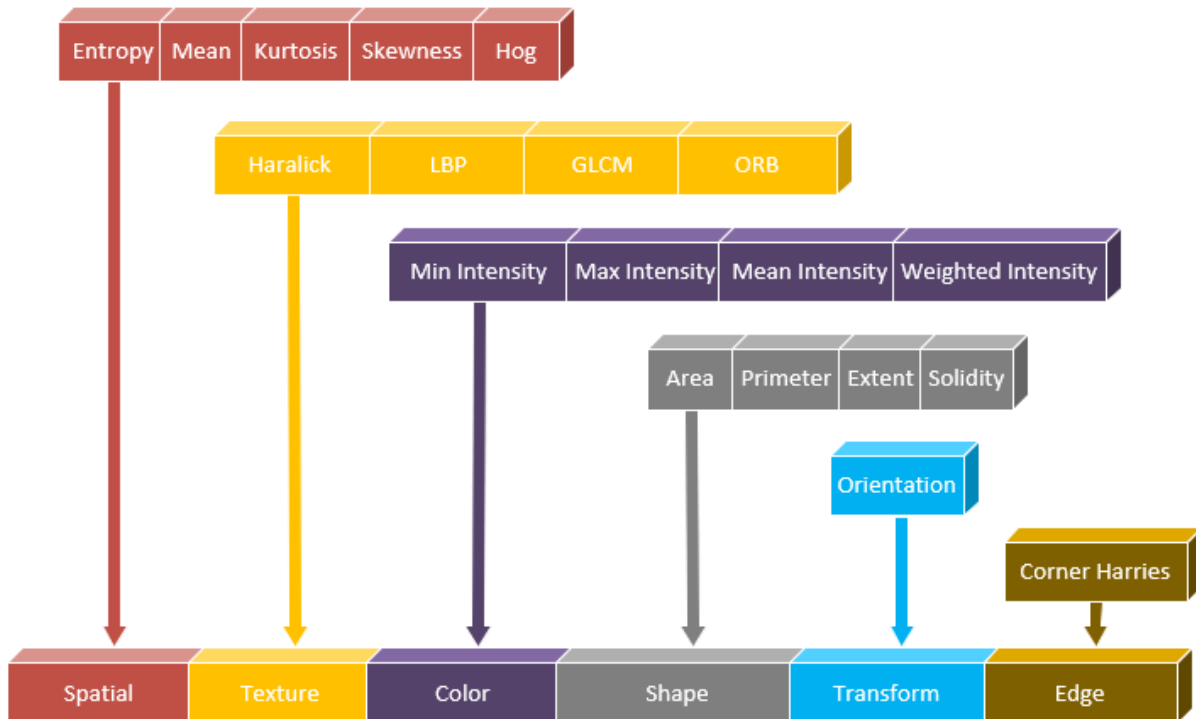


Fig. 3. Placement of features in a vector.

D. Classification

This step employs an ANN to classify ROIs as nodules or non-nodule areas. A classification imbalance issue exists due to the difference in the amount of data between non-nodule areas and nodule ones. The imbalanced classification Markov decision process (ICMDP) method is utilized to formulate a decision-making process that is sequential in nature, in order to deal with the problem of imbalanced classification. RL involves an agent attempting to achieve a high score by taking actions within an environment that lead to an optimal policy. For the suggested model, the agent receives a dataset sample and performs a classification task at each time step. Then, the agent receives the instant feedback from the environment. A correct classification results in a positive score, while an incorrect classification yields a negative score. The optimal policy can be achieved by maximizing the cumulative rewards in the algorithm of RL. Let a set of N samples with corresponding labels be given, denoted as $D = \{(x_1, y_1), (x_2, y_2), (x_3, y_3), \dots, (x_N, y_N)\}$, where x_i is the i -th sample and y_i is its label. The following describes the intended configurations:

- Policy π_θ : Policy π is a function that maps states (S) to actions (A), where $\pi_\theta(s_t)$ represents the action performed in a state s_t . The classifier model with weights θ is referred to as π_θ .
- State s_t : A sample x_t from the dataset D is mapped to each state s_t . The initial state s_1 is represented by the first data x_1 . In order to prevent the model from learning a specific sequence, D is randomized in each episode.
- Action a_t : The action a_t is executed to make a prediction about the label x_t , where the classification is binary, and the possible values of a_t are either 0 or 1. Here, 0 denotes the minority class, while 1 represents the majority class.
- Reward r_t : The reward is based on the performance of the action taken. If the agent performs the correct classification, it receives a positive reward; otherwise, it receives a negative reward. The bonus amount should differ for each class. Calibrated rewards can greatly enhance the model's performance by ensuring that the level of reward is aligned with the action taken. This work specifies the prize for an action using the subsequent formula:

$$r(s_t, a_t, l_t) = \begin{cases} +1, a_t = l_t \text{ and } s_t \in D_P \\ -1, a_t \neq l_t \text{ and } s_t \in D_P \\ \lambda, a_t = l_t \text{ and } s_t \in D_N \\ -\lambda, a_t \neq l_t \text{ and } s_t \in D_N \end{cases} \quad (8)$$

where D_P and D_N show the majority class and minority class. Correctly/incorrectly classifying a sample from the majority class yields a reward of $+\lambda/-\lambda$, where $0 < \lambda < 1$.

- Terminal E: In each training episode, the training process ends at various terminal states. A sequence of state-action pairs $\{(s_1, a_1, y_1), (s_2, a_2, y_2), (s_3, a_3, y_3), \dots, (s_t, a_t, y_t)\}$ from an initial state to a final state is

referred to as an episode. In the suggested model, the end of an episode is determined by either classifying all the training data or by incorrectly classifying a sample from the minority class.

- Transition probability P: The next state, s_{t+1} , is reached by the agent from the current state, s_t , according to the sequence of the data read. The probability of transition is represented as $p(s_{t+1}|s_t, a_t)$.

In deep Q-learning, the agent aims to choose actions to maximize the expected future rewards. Future rewards are worth γ times less in each subsequent time step:

$$R_t = \sum_{t'=t}^T \gamma^{t'-t} r_{t'} \quad (9)$$

where T shows the last time-step of the episode. An episode ends when either all the samples have been classified. Q values, measures of state-action quality, are defined as the expected return of the following strategy π , after seeing state s and taking action a :

$$Q^\pi(s, a) = E[R_t | s_t = s, a_t = a, \pi] \quad (10)$$

The maximum expected reward across all strategies after observing state s and taking action a is the best action-value function:

$$Q^*(s, a) = \max_{\pi} E[R_t | s_t = s, a_t = a, \pi] \quad (11)$$

This function satisfies the Bellman equation, which expresses that the optimal expected return for a given action is equal to the sum of the rewards from the current action and the maximum expected return from future actions at the following time:

$$Q^*(s, a) = E[r + \gamma \max_{a'} Q^*(s', a') | s_t = s, a_t = a] \quad (12)$$

The best action-value function is estimated iteratively utilizing the Bellman equation:

$$Q_{i+1}(s, a) = E[r + \gamma \max_{a'} Q_i(s', a') | s_t = s, a_t = a] \quad (13)$$

During training, after a state s is shown to the network, the network outputs an action a for that state while the environment returns a reward r , and the next state becomes s' . These parameters are embodied in a tuple (s, a, r, s') that is saved into the replay memory, M . Minibatches B of these tuples are selected from the replay memory to perform gradient descent. The loss function is expressed as:

$$L_i(\theta_i) = \sum_{(s, a, r, s') \in B} (y - Q(s, a; \theta_i))^2 \quad (14)$$

where θ indicates the model's weight, and y , shows the estimated target for the Q function. The latter is equal to the reward for the state-action combination plus the discounted maximum future Q value:

$$y = r + \gamma \max_{a'} Q(s', a'; \theta_{k-1}) \quad (15)$$

Of note, the Q value for the terminal state equals zero. The gradient value for the loss function at step i is calculated as follows:

$$\nabla_{\theta_i} L(\theta_i) = -2 \sum_{(s,a,r,s') \in B} (y - Q(s, a; \theta_i)) \nabla_{\theta_i} Q(s, a; \theta_i) \quad (16)$$

By performing a gradient descent step on the loss function, the model weights must be updated to minimize the error:

$$\theta_{i+1} = \theta_i + \alpha \nabla_{\theta_i} Q(s, a; \theta_i) \quad (17)$$

where α represents the learning rate.

E. Localization of Nodule

In the proposed method, sick ROIs, which ANN identifies, are localized by the Otsu thresholding algorithm [65]. Otsu is generally used for segmentation and localization applications [66, 67]. Otsu calculates and evaluates their between-class variation to determine the optimal threshold value. The Otsu shows that maximizing the between-class variance of the segmented classes is equivalent to minimizing the within-class variance. The Otsu segmentation level is acquired by reducing intra-class pixel power or gradually increasing inter-class variance. The inter-class variable specifies the mean between the pixels or classes of pixels [68].

IV. RESULTS AND DISCUSSION

A. Dataset

The Lung Image Database Consortium image collection (LIDC-IDRI) [69] was made by the Foundation for the National Institutes of Health (FNIH) and the Food and Drug Administration (FDA). In this dataset, a thoracic CT scan and a corresponding XML file, including the annotated results done by four radiologists, are included in 1,018 CT scans of 1,010 patients registered. The annotation procedure comprises two stages and seeks to recall all nodules in every CT scan as accurately as possible. In the first step, called the blinded-read step, every radiologist examined scans alone and observed lesions, including “nodule <3 mm” and “non-nodule ≥ 3 mm”. In the second unblinded-read stage, each radiologist checked their marks and decided to be aware of the anonymous marks of different radiologists. In the dataset, 7,371 lesions have been classified as nodules by at least one radiologist; 2,669 of these lesions received at least one “nodule 3 mm” designation from four radiologists, and 928 received four. These 2,669 lesions were given intellectual nodule characteristic ratings and nodule outlines.

B. Results

For this project, Python and the PyTorch framework were used, and the codes were written in a Jupyter notebook. The best model for the LIDC-IDRI dataset was obtained after 50 epochs, and the entire training process lasted for 3.5 hours. The optimal performance of the proposed model hinges on determining the best values for its hyperparameters. This task is not a straightforward one, as it entails exploring a vast search space of potential hyperparameter combinations and conducting numerous experiments to assess their efficacy. It demands significant effort and expertise in designing an

effective search strategy to identify the optimal values for each parameter. To achieve the optimal values, we conducted multiple experiments. A list of the most important parameters used in suggested model is shown in Table I.

The suggested algorithm effectiveness can be determined by comparing the suspicious areas that ANN identified with the real bounding box. For this goal, five algorithms are selected, namely 3D CNN [53], PN-SAMP-M [55], R-CNN [56], DA-Net [57], and MC-CNN [58], for comparison. The evaluation results obtained for the Intersection over Union (IoU) [60] and Hausdorff distance (HD) [70] criteria for the LIDC-IDRI dataset are depicted in Table II. According to the analysis, much research has improved nodule detection performance and achieved relatively excellent results. The IoU value of the MC-CNN model was 0.682, and the 3D CNN model later significantly enhanced it. The offered PN-SAMP-M model achieved an IoU score of 0.711, about 18% better than the previous model. Recent work was on the DA-Net model, which got an IoU score of 0.759. However, the proposed model outperformed the leading algorithm, DA-Net, with an IoU score of 0.825, or by around 20%. Fig. 4 shows examples of nodule detection by these methods. From the figure, the mask bounding box in the proposed model is more matched to that of the ground truth bounding box.

TABLE I. PARAMETER SETTING

Parameter	Value
Number of convolution layers	3
Convolution filters	32, 16, 8
Convolution padding	3 * 3
Convolution stride	2 * 2
Convolution kernel Size	1 * 1
Max-pooling size	2 * 2
Epochs	50
Early stopping	Yes (with patience=5)
Dropout probability	0.4
Batch size	64
Image pixel intensity range	[0, 1]
Image size	100 * 100

TABLE II. COMPARISON OF THE SUGGESTED MODEL WITH OTHER WORKS

Algorithm	IoU	HD
3D CNN [53]	0.683	0.875
PN-SAMP-M [55]	0.711	0.894
R-CNN [56]	0.727	1.136
DA-Net [57]	0.754	1.055
MC-CNN [58]	0.770	1.472
Proposed	0.826	1.618

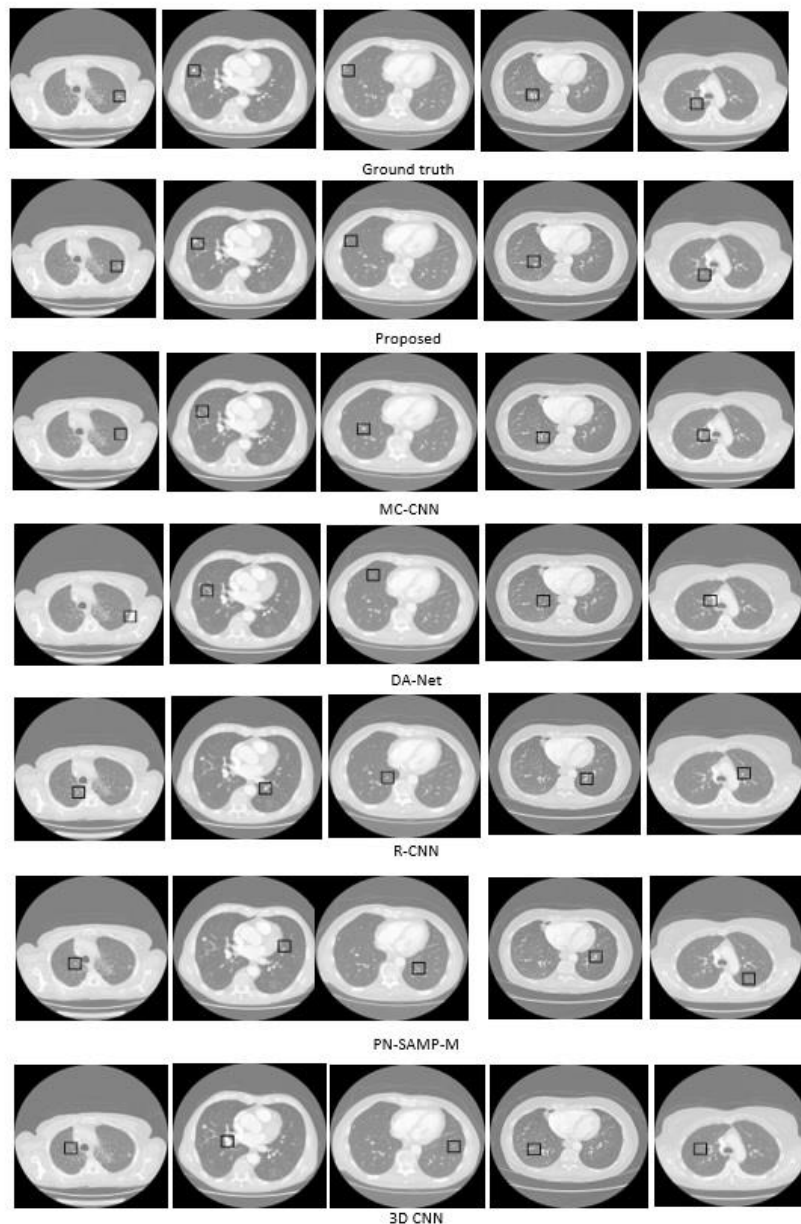


Fig. 4. Examples of nodule detection for methods.

1) *Examples of localizing nodules:* In the proposed algorithm, the suspicious regions detected by the ANN network are given to the Otsu algorithm to extract the localized nodule. Table III shows the results of ten samples of test images with the main images of the lung, single lungs, and localized nodules. Considering all these results shows that the Otsu algorithm localized the nodules well.

2) *Analyze of classifier:* The proposed ANN classifies nodule candidate areas and is a key element in the proposed model's performance. To investigate ANN performance, four models, namely HOUSES-UCB [45], CapsNet [46], MGI-CNN [47], and RFR V-Net [52], were employed for comparison on the LIDC-IDRI dataset. The evaluation criteria utilized are Accuracy, Sensitivity, Precision, F-measure,

Specificity, and G-mean. G-mean and F-measure are valuable metrics for evaluating the effectiveness of imbalanced classification algorithms [71]. G-mean is the geometric mean of sensitivity and precision, and F-measure represents a harmonic mean between recall and precision. As the G-mean and F-measure get a higher score, better performance of the algorithm would be reached. The performance of the proposed ANN, along with RL and the three-deep learning-based models, are compared in Table IV. The ANN model is a classifier that does not use RL for classification, and CNN is a model used instead of ANN. As the results reveal, the ANN+RL model has a more acceptable performance than the rest, which reduces errors by more than 45% in all criteria.

TABLE III. EXAMPLES OF NODULES LOCALIZED BY THE OTSU ALGORITHM

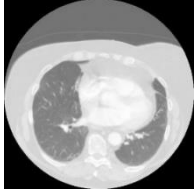
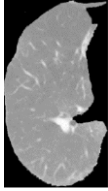
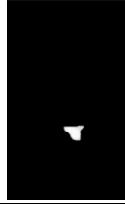
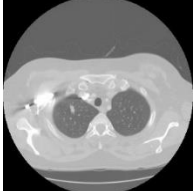
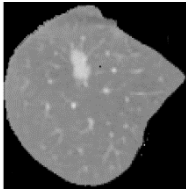
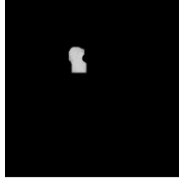
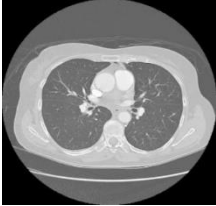
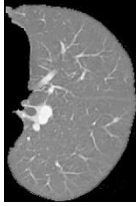

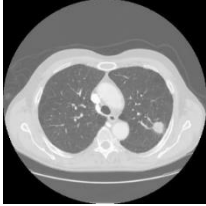
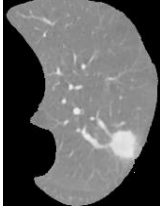

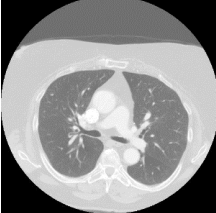
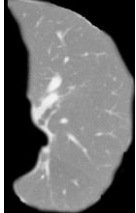

Original Image	Single Lung	localized nodule
		
		
		
		
		

TABLE IV. PERFORMANCE OF VARIOUS CLASSIFIERS

Method	Accuracy	Sensitivity	Precision	F-measure	Specificity	G-mean
HOUSES-UCB	79.11	80.85	90.72	91.52	87.26	82.75
CapsNet	83.00	83.63	91.33	92.35	88.45	83.40
MGI-CNN	85.33	85.71	92.49	93.40	90.02	84.45
RFR V-Net	89.40	90.28	94.72	95.50	91.02	88.48
CNN	84.12	86.23	91.03	91.25	89.15	85.47
ANN	88.13	93.61	95.65	94.61	92.15	86.53
ANN+RL	94.94	96.82	97.91	96.89	95.15	92.90

TABLE V. RESULTS OBTAINED FOR FUZZY ALGORITHMS

Method	IoU	HD
FCM	0.67	1.02
KFCM	0.76	1.56
SAFCM	0.72	1.81
FLICM	0.78	2.01
FRFCM	0.88	2.65

Furthermore, the maximum value of all measures in deep models is relatively different from ANN+RL. For example, by comparing ANN+RL and the second-best model, i.e., RFR V-Net, the difference is about 11% and 10% for the two criteria of F-measure and Recall. The comparison of ANN with ANN+RL shows that the RL trick improved the model by approximately 50%.

3) *Comparison of segmentation methods:* In this section, a comparison of the FRFCM algorithm with other fuzzy-based algorithms is intended. For this purpose, four algorithms, namely FCM [72], KFCM [73], SAFCM [74], and FLICM [75], were selected. The metrics IoU and HD, which are the most widely used for segmentation tasks, were used for evaluation. Table V shows the evaluation results of these methods. FCM had the weakest performance with values of 0.67 and 1.02 for IoU and HD, respectively. The developed algorithms, KFCM and SAFCM, had more power than FCM. Overall, fuzzy methods performed weaker than FRFCM, which outperformed the second-best algorithm, FLICM, with an improvement of roughly 36% for the IoU metric.

To investigate the execution time of algorithms, 20 test data samples were selected and the time spent on them was measured. Table VI shows the average time for these 20 samples. As expected, the time average of the FRFCM algorithm is less than others. Fig. 5 indicates a sample of CT images to highlight the superiority of FRFCM over others. As can be seen, the FCM algorithm did not correctly extract the nodule areas inside the lungs, which severely reduces the system performance since the proposed model's next steps depend on correctly extracting nodules in the segmentation step. Although KFCM performs better, they are unable to extract nodules. FRFCM is the most robust algorithm among the rest.

4) *Exploration of the loss function:* Data imbalances can also be handled using conventional methods, including tweaking data augmentation and loss functions. Among these techniques, the loss function is more important as it can emphasize the minority class. Five functions Balanced Cross-Entropy (BCE), Weighted Cross-Entropy (WCE), Dice Loss (DL), Tversky Loss (TL), and Focal Loss (FL) [76] were chosen to test the effectiveness of the loss functions in the proposed model. In the BCE and WCE loss functions, the positive and negative examples are given equal weight. The FL function can benefit applications using unbalanced data, which helps the model concentrate more on learning complex samples by underweighting the contribution of simple

examples [139]. Table VII displays the evaluation outcomes of these loss functions for the datasets. The FL function outperforms the others as expected, and as a result, it is around 51.16% better than the other loss functions. However, the FL function performs 34% worse than reinforcement learning.

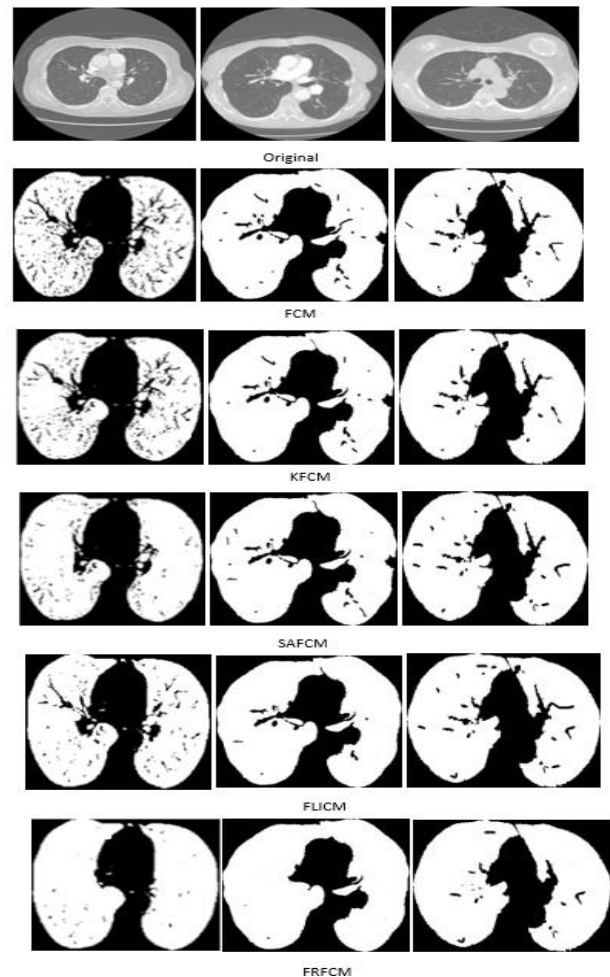


Fig. 5. Examples of lung segmentation by fuzzy algorithms.

TABLE VI. COMPARISON OF EXECUTION TIMES OF METHODS (IN MILLISECOND)

Method	Time
FCM	810
KFCM	405
SAFCM	374
FLICM	328
FRFCM	219

TABLE VII. EFFECTIVENESS OF THE SUGGESTED ANN FOR VARIOUS LOSS FUNCTIONS

Method	Accuracy	Sensitivity	Precision	F-measure	Specificity	G-mean
WCE	83.78	84.25	86.48	86.40	85.03	82.79
BCE	84.47	85.85	87.02	87.79	86.14	83.71
DL	87.09	90.74	90.82	89.63	88.10	85.89
TL	88.25	91.43	92.79	90.20	90.96	87.06
FL	90.55	93.15	94.09	93.19	92.48	89.79

5) *Impact of the reward function:* In the proposed model, rewards of +1 /-1, and $+λ/-λ$ are assigned for correct/incorrect classifications to the majority and minority classes, respectively. $λ$ depends on the relative proportions of the majority to minority samples: the optimal value of $λ$ is expected to decrease as the ratio increases. To investigate the impact of $λ$, the model performance is evaluated with $λ$ initialized using a value from incremental values $\{0,0.1,0.2,0.3,0.4,0.5,0.6,0.7,0.8,0.9,1\}$, while keeping the majority class bonus constant (Fig. 6). At $λ = 0$, the impact of the majority class becomes zeroized; and at $λ = 1$, the relative impacts of both majority and minor classes are equal. Model performance across all metrics peaks at a $λ$ value of 0.3 (increasing from 0 to 0.4, and decreasing from 0.3 to 1. As such, while the effect of the majority class needs to be attenuated by adjusting $λ$, the overall model performance can be degraded by using too low of a value.

6) *Analysis of features extracted by RBM:* The hidden unit in the RBM network fed to ANN is a practical tool containing the compressed data of nodule candidate areas. The additional information is entered into the ANN by increasing the hidden size, which is practically useless. On the other hand, a small hidden size may not be able to hold all the information. To check the effect of the hidden size on the proposed model, six values $\{50, 80, 120, 150, 180, 210\}$ were tried as the hidden size on the model. Fig. 7 displays the results for these metrics. For all metrics, when the hidden size takes the values from the interval $[50, 120]$, the chart moves upward, and from $(120, 210]$, it has a descending movement. Accordingly, the best value for the hidden size is found to be 120.

C. Discussion

This section looks at why the suggested approach produces superior outcomes to other approaches. First of all, suggested model inherits from the hierarchical structure. Although these models may increase the time of diagnosis, they are relatively accurate as they provide each section's analysis process separately.

The proposed model consisted of several parts, each designed for a specific purpose. Two lungs needed to be extracted to reduce the entrance space, and despite the many segmentation methods available, FRFCM was found to be the best option. FRFCM was selected due to its short implementation time and acceptable results obtained in other articles, and its superiority over other algorithms was confirmed in Tables V and VI. Additionally, unlike different algorithms, FRFCM completely extracted all the holes in terms of schematic output, demonstrating its stability against various noise and other image disturbances (see Fig. 5). In the following steps, it was unnecessary to utilize a lung that did not include a nodule. Among deep learning structures for classification, CNN was the best architecture, which required little pre-processing compared to others. Whereas, in previous designs, filters were typically hand-engineered, CNN learned these filters firmly. Therefore, the first stage alone could diagnose lung diseases that might be hidden from the physician.

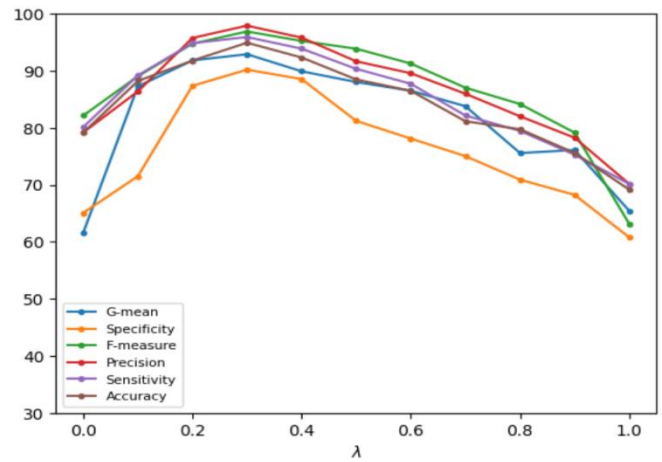


Fig. 6. Performance metrics plotted vs. the value of λ in the reward function.

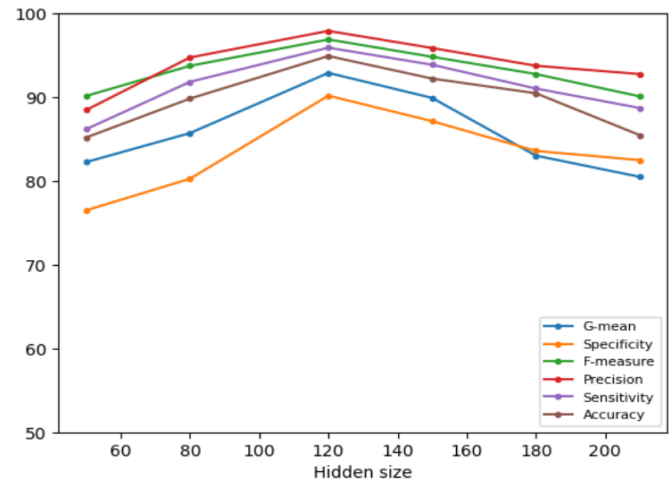


Fig. 7. Performance metrics plotted vs. the hidden size in RBM.

To reduce the input space further, the adaptive thresholding method was chosen as the best algorithm to select ROIs that are more likely to be nodules. This algorithm works well because it compares a pixel with the pixels around the contrast lines and prevents soft gradient changes. Moreover, another advantage is that only one image pass is needed.

One of the proposed algorithm's steps was selecting and extracting ROIs for classification. Although CNNs are one of the best models for classification, they cannot be helpful for tiny areas. In the experiments, CNN is used with various architectures as a classifier and reported the best result in Table IV. As can be seen, it works weaker than ANN. On the other hand, due to the nature of deep learning, the leading network is multi-layered, so some features are lost during the extraction and transfer process to the lower layer. In particular, overfitting may occur due to the extraction of many features. These problems are exacerbated if the amount of data is small. Therefore, the traditional feature selection process can be one of the critical options for selecting basic features with little data and achieving high accuracy. But the presence of unrelated and redundant features reduces the performance of machine learning models. For this purpose, an RBM that can encode any distribution and is computationally efficient was applied. Moreover, activations of the hidden layer can be used as input

in deeper models. The performance of the model is also affected by the size of the hidden layer, for which there is generally no rule for the number of hidden layers and accuracy. As shown in Fig. 7, better performance was obtained by setting the size to 120.

But the most important and innovative part of the proposed method was the classification of ROIs with ANN, which was an imbalanced problem due to a large amount of majority class data. From the results, it was confirmed that reinforcement learning applied to the classification could essentially solve it. On the other hand, it is hypothesized that the reinforcement learning method used in this study can be utilized by all classifiers experiencing imbalance to address this issue.

One potential limitation of the proposed model is its computational intensity, which may be due to the use of multiple algorithms, such as FRFCM, CNN, adaptive thresholding, RBM, ANN, and Otsu thresholding. As a result, the processing time required for analyzing a large number of CT images may increase. Another limitation is the possibility of class imbalance, as sick ROIs are less common than healthy ones, which may decrease the performance of the ANN. Although the reinforcement learning-based algorithm is used to address this issue, it may not always be fully effective. Furthermore, the accuracy of the proposed model may be dependent on the quality of the CT images used for analysis. The model's accuracy may decrease if the images have poor resolution or are affected by image artifacts or noise. Lastly, the proposed model was evaluated using the LIDC-IDRI dataset, and its performance may vary when applied to other datasets or in clinical settings. Therefore, further testing and validation are necessary to determine the model's robustness and generalizability.

V. CONCLUSION

This paper presented a hybrid method to recognize the pulmonary nodules in CT lung images. The proposed method's structure was composed of five different steps. First, the FRFCM algorithm is applied, which developed fast and robust to segment CT images, followed by a CNN to identify the sick lung. Then, the adaptive thresholding algorithm is performed to detect suspected ROIs from sick lungs identified by CNN. Next, some statistical features are determined from every ROI, and then an RBM is hired as a feature extractor that extracts wealthy features. After that, an ANN is utilized to classify ROIs as nodule or non-nodule areas. Finally, sick ROIs are localized by the Otsu thresholding algorithm. Naturally, sick ROIs are less than healthy ones, resulting in an imbalanced classification that reduces ANN performance. To shield this problem, RL is applied, which frames the training process as a sequential decision-making step. At each stage, the agent gets an example and categorizes it. The agent gets a reward from the environment for each categorization act in which the minority class receives a larger reward than the majority class. Finally, the agent discovers an optimal policy with a specific reward function and a supportive learning environment. Several experiments are designed to investigate the parts of the suggested model on the LIDC-IDRI dataset and standard performance metrics. Experimental findings showed that the suggested model performs better than other competitors.

In future work, it is planned to use 3D processing instead of 2D, which may increase the effectiveness of the proposed solution. Additionally, focus will be given to feature selection or extraction to improve the speed and accuracy of the suggested method.

REFERENCES

- [1] K.-J. Wang, J.-L. Chen, K.-M. Wang, Medical expenditure estimation by Bayesian network for lung cancer patients at different severity stages, *Computers in biology and medicine*, 106, pp. 97-105, 2019.
- [2] S. Afaghi, F.E. Tarki, F.S. Rahimi, S. Besharat, S. Mirhaidari, A. Karimi, N.M. Alamdari, Prevalence and clinical outcomes of vitamin D deficiency in COVID-19 hospitalized patients: a retrospective single-center analysis, *The Tohoku Journal of Experimental Medicine*, 255, pp. 127-134, 2021.
- [3] N. Khosravan, H. Celik, B. Turkbey, E.C. Jones, B. Wood, U. Bagci, A collaborative computer aided diagnosis (C-CAD) system with eye-tracking, sparse attentional model, and deep learning, *Medical image analysis*, 51, pp. 101-115, 2019.
- [4] M.S. Hakemi, A.A. Nassiri, A. Nobakht, M. Mardani, I.A. Darazam, M. Parsa, M.M. Miri, R. Shahrani, A.A. Koomleh, K. Entezarmahdi, Benefit of hemoadsorption therapy in patients suffering sepsis-associated acute kidney injury: a case series, *Blood Purification*, 51, pp. 823-830, 2022.
- [5] D. Riquelme, M.A. Akhloufi, Deep learning for lung cancer nodules detection and classification in CT scans, *AI*, 1, pp. 28-67, 2020.
- [6] A.Q. Al-Faris, U.K. Ngah, N.A.M. Isa, I.L. Shuaib, Breast MRI tumour segmentation using modified automatic seeded region growing based on particle swarm optimization image clustering, *Soft Computing in Industrial Applications*, Springer, 2014, pp. 49-60.
- [7] J.C. Bezdek, Pattern recognition with fuzzy objective function algorithms, Springer Science & Business Media 2013.
- [8] A.K. Jain, Data clustering: 50 years beyond K-means, *Pattern recognition letters*, 31, pp. 651-666, 2010.
- [9] T. Lei, X. Jia, Y. Zhang, L. He, H. Meng, A.K. Nandi, Significantly fast and robust fuzzy c-means clustering algorithm based on morphological reconstruction and membership filtering, *IEEE Transactions on Fuzzy Systems*, 26, pp. 3027-3041, 2018.
- [10] N. Esfandiari, M.R. Babavalian, A.-M.E. Moghadam, V.K. Tabar, Knowledge discovery in medicine: Current issue and future trend, *Expert Systems with Applications*, 41, pp. 4434-4463, 2014.
- [11] S.L.A. Lee, A.Z. Kouzani, E.J. Hu, Automated detection of lung nodules in computed tomography images: a review, *Machine vision and applications*, 23, pp. 151-163, 2012.
- [12] F. Shaukat, G. Raja, A.F. Frangi, Computer-aided detection of lung nodules: a review, *Journal of Medical Imaging*, 6, p. 020901, 2019.
- [13] A. Nibali, Z. He, D. Wollersheim, Pulmonary nodule classification with deep residual networks, *International journal of computer assisted radiology and surgery*, 12, pp. 1799-1808, 2017.
- [14] N. Zhang, S. Ding, J. Zhang, Y. Xue, An overview on restricted Boltzmann machines, *Neurocomputing*, 275, pp. 1186-1199, 2018.
- [15] M. Moradi, M. Samwald, Deep Learning, Natural Language Processing, and Explainable Artificial Intelligence in the Biomedical Domain, arXiv preprint arXiv:2202.12678, 2022.
- [16] H. Han, W.-Y. Wang, B.-H. Mao, Borderline-SMOTE: a new over-sampling method in imbalanced data sets learning, *International conference on intelligent computing*, Springer, pp. 878-887, 2005.
- [17] J. Chen, C.-A. Tsai, H. Moon, H. Ahn, J. Young, C.-H. Chen, Decision threshold adjustment in class prediction, SAR and QSAR in Environmental Research, 17, pp. 337-352, 2006.
- [18] C. Huang, Y. Li, C.C. Loy, X. Tang, Learning deep representation for imbalanced classification, *Proceedings of the IEEE conference on computer vision and pattern recognition*, pp. 5375-5384, 2016.
- [19] A. Naik, D.R. Edla, Lung Nodule Classification on Computed Tomography Images Using Deep Learning, *Wireless Personal Communications*, 116, pp. 655-690, 2021.

- [20] E. Dandil, A computer-aided pipeline for automatic lung cancer classification on computed tomography scans, *Journal of healthcare engineering*, 2018, 2018.
- [21] S. Ozekes, A.Y. Camurcu, Automatic lung nodule detection using template matching, *International Conference on Advances in Information Systems*, Springer, pp. 247-253, 2006.
- [22] H. Wu, T. Sun, J. Wang, X. Li, W. Wang, D. Huo, P. Lv, W. He, K. Wang, X. Guo, Combination of radiological and gray level co-occurrence matrix textural features used to distinguish solitary pulmonary nodules by computed tomography, *Journal of digital imaging*, 26, pp. 797-802, 2013.
- [23] J. Kuruvilla, K. Gunavathi, Lung cancer classification using neural networks for CT images, *Computer methods and programs in biomedicine*, 113, pp. 202-209, 2014.
- [24] F.V. Farahani, A. Ahmadi, M.H.F. Zarandi, Hybrid intelligent approach for diagnosis of the lung nodule from CT images using spatial kernelized fuzzy c-means and ensemble learning, *Mathematics Computers in Simulation*, 149, pp. 48-68, 2018.
- [25] M.A. Khan, S. Rubab, A. Kashif, M.I. Sharif, N. Muhammad, J.H. Shah, Y.-D. Zhang, S.C. Satapathy, Lung cancer classification from CT images: An integrated design of contrast based classical features fusion and selection, *Pattern Recognition Letters*, 129, pp. 77-85, 2020.
- [26] M.S. Sartakhti, M.J.M. Kahaki, S.V. Moravvej, M. javadi Joortani, A. Bagheri, Persian language model based on BiLSTM model on COVID-19 corpus, *2021 5th International Conference on Pattern Recognition and Image Analysis (IPRIA)*, IEEE, pp. 1-5, 2021.
- [27] S.V. Moravvej, A. Mirzaei, M. Safayani, Biomedical text summarization using Conditional Generative Adversarial Network (CGAN), *arXiv preprint arXiv:2110.11870*, 2021.
- [28] S.V. Moravvej, M.J.M. Kahaki, M.S. Sartakhti, A. Mirzaei, A method based on attention mechanism using bidirectional long-short term memory (BLSTM) for question answering, *2021 29th Iranian Conference on Electrical Engineering (ICEE)*, IEEE, pp. 460-464, 2021.
- [29] Z. SobhaniNia, N. Karimi, P. Khadivi, R. Roshandel, S. Samavi, Brain Tumor Classification Using Medial Residual Encoder Layers, *arXiv preprint arXiv:2011.00628*, 2020.
- [30] Z. Sobhaninia, N. Karimi, P. Khadivi, S. Samavi, Brain Tumor Classification by Cascaded Multiscale Multitask Learning Framework Based on Feature Aggregation, *arXiv preprint arXiv:2112.14320*, 2021.
- [31] G. Peeters, G. Richard, *Deep Learning for Audio and Music*, Springer, 2021.
- [32] S.V. Moravvej, M. Joodaki, M.J.M. Kahaki, M.S. Sartakhti, A method Based on an Attention Mechanism to Measure the Similarity of two Sentences, *2021 7th International Conference on Web Research (ICWR)*, IEEE, pp. 238-242, 2021.
- [33] T. Iqbal, S. Qureshi, The survey: Text generation models in deep learning, *Journal of King Saud University-Computer and Information Sciences*, 2020.
- [34] S. Moravvej, M. Maleki Kahaki, M. Salimi Sartakhti, M. Joodaki, Efficient GAN-based Method for Extractive Summarization, *Journal of Electrical and Computer Engineering Innovations (JECEI)*, 2021.
- [35] S.V. Moravvej, S.J. Mousavirad, M.H. Moghadam, M. Saadatmand, An LSTM-Based Plagiarism Detection via Attention Mechanism and a Population-Based Approach for Pre-training Parameters with Imbalanced Classes, *International Conference on Neural Information Processing*, Springer, pp. 690-701, 2021.
- [36] S.V. Moravvej, S.J. Mousavirad, D. Oliva, G. Schaefer, Z. Sobhaninia, An Improved DE Algorithm to Optimise the Learning Process of a BERT-based Plagiarism Detection Model, *2022 IEEE Congress on Evolutionary Computation (CEC)*, IEEE, pp. 1-7, 2022.
- [37] S.V. Moravvej, R. Alizadehsani, S. Khanam, Z. Sobhaninia, A. Shoeibi, F. Khozeimeh, Z.A. Sani, R.-S. Tan, A. Khosravi, S. Nahavandi, RLMD-PA: a reinforcement learning-based myocarditis diagnosis combined with a population-based algorithm for pretraining weights, *Contrast Media & Molecular Imaging*, 2022, 2022.
- [38] S. Danaei, A. Bostani, S.V. Moravvej, F. Mohammadi, R. Alizadehsani, A. Shoeibi, H. Alinejad-Rokny, S. Nahavandi, Myocarditis Diagnosis: A Method using Mutual Learning-Based ABC and Reinforcement Learning, *2022 IEEE 22nd International Symposium on Computational Intelligence and Informatics and 8th IEEE International Conference on Recent Achievements in Mechatronics, Automation, Computer Science and Robotics (CINTI-MACRo)*, IEEE, pp. 000265-000270, 2022.
- [39] H. Cao, H. Liu, E. Song, G. Ma, X. Xu, R. Jin, T. Liu, C.-C. Hung, A two-stage convolutional neural networks for lung nodule detection, *IEEE journal of biomedical and health informatics*, 24, pp. 2006-2015, 2020.
- [40] Z. Ali, A. Irtaza, M. Maqsood, An efficient U-Net framework for lung nodule detection using densely connected dilated convolutions, *The Journal of Supercomputing*, 78, pp. 1602-1623, 2022.
- [41] S. Vakilian, S.V. Moravvej, A. Faniyan, Using the artificial bee colony (ABC) algorithm in collaboration with the fog nodes in the Internet of Things three-layer architecture, *2021 29th Iranian Conference on Electrical Engineering (ICEE)*, IEEE, pp. 509-513, 2021.
- [42] S. Vakilian, S.V. Moravvej, A. Faniyan, Using the cuckoo algorithm to optimizing the response time and energy consumption cost of fog nodes by considering collaboration in the fog layer, *2021 5th International Conference on Internet of Things and Applications (IoT)*, IEEE, pp. 1-5, 2021.
- [43] G. Zhang, Z. Yang, L. Gong, S. Jiang, L. Wang, Classification of benign and malignant lung nodules from CT images based on hybrid features, *Physics in Medicine and Biology*, 64, p. 125011, 2019.
- [44] D. Blanc, V. Racine, A. Khalil, M. Deloche, J.-A. Broyelle, I. Hammouamri, E. Sinitambirivoutin, M. Fiammante, E. Verdier, T. Besson, Artificial intelligence solution to classify pulmonary nodules on CT, *Diagnostic interventional imaging*, 101, pp. 803-810, 2020.
- [45] M. Zhang, H. Li, J. Lyu, S.H. Ling, S. Su, Multi-level CNN for lung nodule classification with Gaussian Process assisted hyperparameter optimization, *arXiv preprint arXiv:00276*, 2019.
- [46] A. Mobiny, H. Van Nguyen, Fast capsnet for lung cancer screening, *International Conference on Medical Image Computing and Computer-Assisted Intervention*, Springer, pp. 741-749, 2018.
- [47] B.-C. Kim, J.S. Yoon, J.-S. Choi, H.-I. Suk, Multi-scale gradual integration CNN for false positive reduction in pulmonary nodule detection, *Neural Networks*, 115, pp. 1-10, 2019.
- [48] O. Ozdemir, B. Woodward, A.A. Berlin, Propagating uncertainty in multi-stage bayesian convolutional neural networks with application to pulmonary nodule detection, *arXiv preprint arXiv:1712.00497*, 2017.
- [49] W. Zhu, Y.S. Vang, Y. Huang, X. Xie, Deepem: Deep 3d convnets with em for weakly supervised pulmonary nodule detection, *International Conference on Medical Image Computing and Computer-Assisted Intervention*, Springer, pp. 812-820, 2018.
- [50] Q. Dou, H. Chen, L. Yu, J. Qin, P.-A. Heng, Multilevel contextual 3-D CNNs for false positive reduction in pulmonary nodule detection, *IEEE Transactions on Biomedical Engineering*, 64, pp. 1558-1567, 2016.
- [51] H. Jiang, H. Ma, W. Qian, M. Gao, Y. Li, An automatic detection system of lung nodule based on multigroup patch-based deep learning network, *IEEE journal of biomedical and health informatics*, 22, pp. 1227-1237, 2017.
- [52] S. Dodia, A. Basava, M. Padukudru Anand, A novel receptive field-regularized V-net and nodule classification network for lung nodule detection, *International Journal of Imaging Systems and Technology*, 2022.
- [53] X. Huang, J. Shan, V. Vaidya, Lung nodule detection in CT using 3D convolutional neural networks, *2017 IEEE 14th International Symposium on Biomedical Imaging (ISBI 2017)*, IEEE, pp. 379-383, 2017.
- [54] S.M. Ganji, M. Tehranchi, A. Ehterami, H. Semyari, F. Taleghani, M. Habibzadeh, M.H. Tayeed, N. Mehrnia, A. Karimi, M. Salehi, Bone tissue engineering via application of a PCL/Gelatin/Nanoclay/Hesperetin 3D nanocomposite scaffold, *Journal of Drug Delivery Science and Technology*, 76, p. 103704, 2022.
- [55] B. Wu, Z. Zhou, J. Wang, Y. Wang, Joint learning for pulmonary nodule segmentation, attributes and malignancy prediction, *2018 IEEE 15th International Symposium on Biomedical Imaging (ISBI 2018)*, IEEE, pp. 1109-1113, 2018.
- [56] X. Huang, W. Sun, T.-L.B. Tseng, C. Li, W. Qian, Fast and fully-automated detection and segmentation of pulmonary nodules in thoracic

- CT scans using deep convolutional neural networks, *Computerized Medical Imaging and Graphics*, 74, pp. 25-36, 2019.
- [57] M. Maqsood, S. Yasmin, I. Mehmood, M. Bukhari, M. Kim, An Efficient DA-Net Architecture for Lung Nodule Segmentation, *Mathematics*, 9, p. 1457, 2021.
- [58] W. Shen, M. Zhou, F. Yang, D. Yu, D. Dong, C. Yang, Y. Zang, J. Tian, Multi-crop convolutional neural networks for lung nodule malignancy suspiciousness classification, *Pattern Recognition*, 61, pp. 663-673, 2017.
- [59] M.N. Mughal, W. Ikram, Early lung cancer detection by classifying chest CT images: a survey, 8th International Multitopic Conference, 2004. Proceedings of INMIC 2004., IEEE, pp. 67-72, 2004.
- [60] H. Rezatofghi, N. Tsoi, J. Gwak, A. Sadeghian, I. Reid, S. Savarese, Generalized intersection over union: A metric and a loss for bounding box regression, *Proceedings of the IEEE/CVF Conference on Computer Vision and Pattern Recognition*, pp. 658-666, 2019.
- [61] F.V. Farahani, A. Ahmadi, M.H.F. Zarandi, Hybrid intelligent approach for diagnosis of the lung nodule from CT images using spatial kernelized fuzzy c-means and ensemble learning, *Mathematics and Computers in Simulation*, 149, pp. 48-68, 2018.
- [62] C. Fuchs, S. Heuel, Feature extraction, *Second Course in Digital Photogrammetry*, pp. 3-1, 1995.
- [63] F. Afza, M.A. Khan, M. Sharif, A. Rehman, Microscopic skin laceration segmentation and classification: A framework of statistical normal distribution and optimal feature selection, *Microscopy research technique*, 82, pp. 1471-1488, 2019.
- [64] B. Remeseiro, V. Bolon-Canedo, A review of feature selection methods in medical applications, *Computers in biology and medicine*, 112, p. 103375, 2019.
- [65] M. Sharif, M.A. Khan, M. Faisal, M. Yasmin, S.L. Fernandes, A framework for offline signature verification system: Best features selection approach, *Pattern Recognition Letters*, 2018.
- [66] Y. Tan, K. Lu, J. Xue, An Automated Lung Nodule Segmentation Method Based On Nodule Detection Network and Region Growing, *Proceedings of the ACM Multimedia Asia*, 2019, pp. 1-6.
- [67] R. Mastouri, H. Neji, S. Hantous-Zannad, N. Khelifa, A morphological operation-based approach for Sub-pleural lung nodule detection from CT images, 2018 IEEE 4th Middle East Conference on Biomedical Engineering (MECBME), IEEE, pp. 84-89, 2018.
- [68] W. Abbas, K.B. Khan, M. Aqeel, M.A. Azam, M.H. Ghouri, F.H. Jaskani, Lungs Nodule Cancer Detection Using Statistical Techniques, 2020 IEEE 23rd International Multitopic Conference (INMIC), IEEE, pp. 1-6, 2020.
- [69] L.M. Pehrson, M.B. Nielsen, C. Ammitzbøl Lauridsen, Automatic pulmonary nodule detection applying deep learning or machine learning algorithms to the LIDC-IDRI database: a systematic review, *Diagnostics*, 9, p. 29, 2019.
- [70] D.P. Huttenlocher, G.A. Klanderman, W.J. Rucklidge, Comparing images using the Hausdorff distance, *IEEE Transactions on pattern analysis and machine intelligence*, 15, pp. 850-863, 1993.
- [71] Q. Gu, L. Zhu, Z. Cai, Evaluation measures of the classification performance of imbalanced data sets, *International symposium on intelligence computation and applications*, Springer, pp. 461-471, 2009.
- [72] J.C. Bezdek, R. Ehrlich, W. Full, FCM: The fuzzy c-means clustering algorithm, *Computers & geosciences*, 10, pp. 191-203, 1984.
- [73] Y. Ding, X. Fu, Kernel-based fuzzy c-means clustering algorithm based on genetic algorithm, *Neurocomputing*, 188, pp. 233-238, 2016.
- [74] K.-S. Chuang, H.-L. Tzeng, S. Chen, J. Wu, T.-J. Chen, Fuzzy c-means clustering with spatial information for image segmentation, *computerized medical imaging and graphics*, 30, pp. 9-15, 2006.
- [75] M. Lavanya, P.M. Kannan, Lung lesion detection in CT scan images using the fuzzy local information cluster means (FLICM) automatic segmentation algorithm and back propagation network classification, *Asian Pacific journal of cancer prevention: APJCP*, 18, p. 3395, 2017.
- [76] S. Jadon, A survey of loss functions for semantic segmentation, 2020 IEEE Conference on Computational Intelligence in Bioinformatics and Computational Biology (CIBCB), IEEE, pp. 1-7, 2020.